AD

TECHNICAL REPORT ARCCB-TR-00004

DYNAMIC SCALING IN CELLULAR AUTOMATA SIMULATIONS OF DEPOSITION PROCESSES

MARK JOHNSON

MARCH 2000

US ARMY ARMAMENT RESEARCH,
DEVELOPMENT AND ENGINEERING CENTER
CLOSE COMBAT ARMAMENTS CENTER
BENÉT LABORATORIES
WATERVLIET, N.Y. 12189-4050

DISCLAIMER

The findings in this report are not to be construed as an official Department of the Army position unless so designated by other authorized documents.

The use of trade name(s) and/or manufacturer(s) does not constitute an official endorsement or approval.

DESTRUCTION NOTICE

For classified documents, follow the procedures in DoD 5200.22-M, Industrial Security Manual, Section II-19, or DoD 5200.1-R, Information Security Program Regulation, Chapter IX.

For unclassified, limited documents, destroy by any method that will prevent disclosure of contents or reconstruction of the document.

For unclassified, unlimited documents, destroy when the report is no longer needed. Do not return it to the originator.

REPORT DOCUMENTATION PAGE

Form Approved
OMB No. 0704-0188

1. AGENCY USE ONLY (Leave blank)	2. REPORT DATE	3. REPORT TYPE AND DATES COVERED
	March 2000	Final

4. TITLE AND SUBTITLE

DYNAMIC SCALING IN CELLULAR AUTOMATA SIMULATIONS OF DEPOSITION PROCESSES

5. FUNDING NUMBERS

AMCMS No. 6227.20.9471.2

6. AUTHOR(S)

Mark Johnson

7. PERFORMING ORGANIZATION NAME(S) AND ADDRESS(ES)

U.S. Army ARDEC
Benet Laboratories, AMSTA-AR-CCB-O
Watervliet, NY 12189-4050

8. PERFORMING ORGANIZATION REPORT NUMBER

ARCCB-TR-00004

9. SPONSORING / MONITORING AGENCY NAME(S) AND ADDRESS(ES)

U.S. Army ARDEC
Close Combat Armaments Center
Picatinny Arsenal, NJ 07806-5000

10. SPONSORING / MONITORING AGENCY REPORT NUMBER

11. SUPPLEMENTARY NOTES

To be presented at the High Performance Computing Symposium 2000, Washington, DC, 16-20 April 2000.
To be published in proceedings of the symposium.

12a. DISTRIBUTION / AVAILABILITY STATEMENT

Approved for public release; distribution unlimited.

12b. DISTRIBUTION CODE

13. ABSTRACT *(Maximum 200 words)*

Cellular automata simulations can be used to capture many of the essential features of processes that are difficult to model. They are particularly useful in the study of nonlinear dynamical systems that have complex continuous solutions. In this study, cellular automata models have been employed to investigate the nature of the vapor deposition process by exploring the natural evolution of dynamical dissipative systems using self-organized critical system analysis and spatial scaling measures. A new numerical technique is introduced to analyze the intrinsic structure of evolving surface topography in an effort to better understand the dynamics of the growth processes. This technique is being used to validate the integrity of deposition models through a comparative analysis with experimental data and to determine if a correlation exists between intrinsic surface structure and parameters controlling the deposition process.

14. SUBJECT TERMS	15. NUMBER OF PAGES
Image Processing, Fractals, Cellular Automata	13
	16. PRICE CODE

17. SECURITY CLASSIFICATION OF REPORT	18. SECURITY CLASSIFICATION OF THIS PAGE	19. SECURITY CLASSIFICATION OF ABSTRACT	20. LIMITATION OF ABSTRACT
UNCLASSIFIED	UNCLASSIFIED	UNCLASSIFIED	UL

TABLE OF CONTENTS

TABLES

LIST OF ILLUSTRATIONS

ACKNOWLEDGEMENTS

The author would like to thank Mr. Royce Soanes for his valuable assistance in developing the spline solutions that are used in the measurement of the scaling parameters.

INTRODUCTION

The notion of self-organized critical systems has been introduced by Bak *et al.* (ref 1) to provide a consistent explanation for the fractal spatial structures, power law distributions, and flicker noise commonly observed in spatially extended-driven dynamical systems. They have proposed a deposition model with a geometric configuration that evolves toward a critical form. The critical state is an attractor for the dynamics of the system, and the model demonstrates how complex fractal surfaces evolve from simple system dynamics.

APPROACH

The cellular automata employed in this study are based on a two-dimensional regular lattice of cells using the rules given by Kadanoff *et al.* (ref 2). The basic variable is $z(i,j)$, where (i,j) are the spatial indices and z represents the height of the lattice. The system is initialized to a planar surface, $z(i,j) = 0$. Particles are added at random locations $z(i,j)$ such that $z(i,j) \rightarrow z(i,j) + 1$ as long as the sites are stable. After a particle is added and after particle rearrangements, the stability of all lattice sites is determined by $z(i,j)$ and the nearest neighbor z values. In the model treated here, a site becomes unstable when

$$\sum_{k=-1}^{k=1}\{z(i,j)-z(i,j-k))H(z(i,j)-z(i,j-k))+ (z(i,j)-z(i-k,j))H(z(i,j)-z(i-k,j))\}>\sigma_c \qquad (1)$$

where H is the Heaviside function and σ_c is the stability parameter. If site (i,j) becomes unstable, $z(i,j)$ is reduced by $\Delta z(i,j)$, where $\Delta z(i,j) =$

$$\sum_{k=-1}^{k=1}\{H(z(i,j)-z(i,j-k))+H(z(i,j)-z(i-k,j))\} \qquad (2)$$

The height of the corresponding nearest neighbor cells is incremented by 1 if their height is less than $z(i,j)$. If all sites are stable, a new particle is added to the system. The boundaries are periodic and the local rule is applied recursively to the cells whose state is affected by the unstable site. The diffusion process continues until there are no more unstable sites, but no new particles are added until the lattice stabilizes. The number of sites that are changed as the lattice reorganizes after a particle is added is the size of an avalanche, and the total number of particles that have been added to the system is denoted n.

The avalanches have been extensively explored (refs 1-4), and it has been demonstrated that avalanche sizes have the form of cutoff hyperbolic distributions. However, quantitative analysis of the geometric scaling properties of the evolving automata structures has been limited. One study by Meisel and Johnson (ref 5) has explored the structures in terms of self-similar fractals, and it has been shown that there is a monotonic increase in the Hausdorf-Besokovitch dimension D with increasing σ_c.

However, the nature of the deposition process and the cellular automata models suggest that the resulting surface morphology belongs to a class of fractals called *surface fractals* (ref 6), which are usually measured in terms of self-affine fractal parameters (ref 7). Self-affine fractals are statistically invariant under anisotropic dilations, whereas self-similar fractals are statistically invariant under isotropic dilations (ref 8). The simulations being investigated in this study pertain to surfaces in E^3 and are characterized by statistical invariance under transformations of the form

$$\{x,y,z\} \rightarrow \{\lambda x, \lambda y, \lambda^H z\} \tag{3}$$

where the Hurst exponent, H, describes the anisotropic scaling. In a more general case, the y coordinate would have a coefficient λ^K, and in the case of self-similar fractals, H would have a value of 1. The invariance expressed in equation (3) implies that any point on a self-affine surface can be represented in the form $\{\mathbf{r}, h(\mathbf{r})\}$, where the height function $h(\mathbf{r})$ is a single-valued function of $\mathbf{r} \equiv \{x,y\} \in \Sigma$. Equation (3) applies over a scaling range that is measured in terms of a parallel correlation length, $\xi_{//}$. The parallel correlation length is the distance beyond which there is no correlation in heights between points on the surface. The roughness of the surface (σ) is defined in terms of the perpendicular correlation length, $\xi_{\perp}$, which is related to the rms variations in $h(\mathbf{r})$. Assuming a homogenous, self-affine, surface structure, the height correlation function is given by (ref 7)

$$C_h(\mathbf{r}) = \left\langle \left[h(\mathbf{r}_0 + \mathbf{r}) - h(\mathbf{r}_0)\right]^2 \right\rangle_{\mathbf{r}_0} \tag{4}$$

The Hurst exponent H is defined by the small $\mathbf{r}$ variations in $C_h(\mathbf{r})$, i.e.,

$$H = \tfrac{1}{2}\, d(\ln(C_h(\mathbf{r}))/d(\ln(\mathbf{r}))(\mathbf{r} << \xi_{//}) \tag{5}$$

where the range of $\mathbf{r}$ corresponding to the linear range in $C_h(\mathbf{r})$ is referred to as the scaling range. Beyond the scaling range at large $\mathbf{r}$, the elevations become uncorrelated and $C_h(\mathbf{r})$ is given by

$$C_h(\mathbf{r}) \rightarrow 2\sigma^2 (\mathbf{r} >> \xi_{//}) \tag{6}$$

where σ is the surface roughness and $2\sigma^2$ is referred to as the perpendicular correlation length, $\xi_{\perp}$. Figure 1 shows the double logarithmic plot of $C_h(\mathbf{r})$ versus $\mathbf{r}$ for a self-affine fractal model.

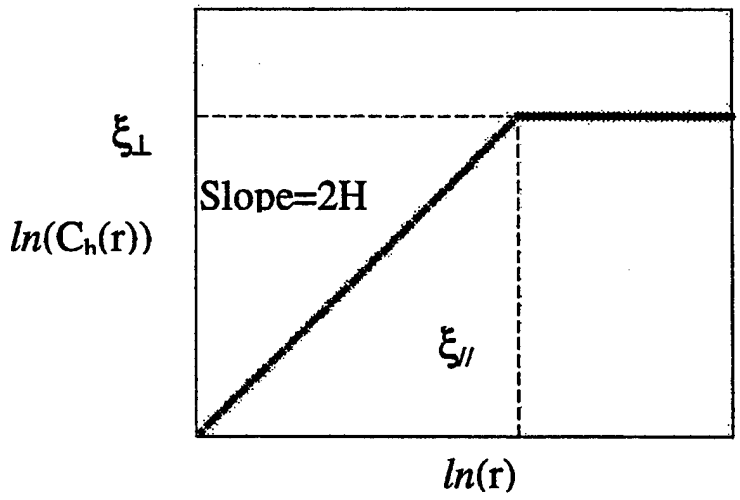

Figure 1. $C_h(r)$ for a self-affine fractal model.

MEASURING THE SCALING PARAMETERS

Figures 2a and b show the evolving surface geometry of a cellular automaton model with $\sigma_c = 9$. Figure 3 shows the height correlation function corresponding to the surface after 10^7 iterations. Although the height correlation function has the functional form of a self-affine fractal model, estimates of $\xi_{//}$ and H depend on the range of data used to fit the linear region.

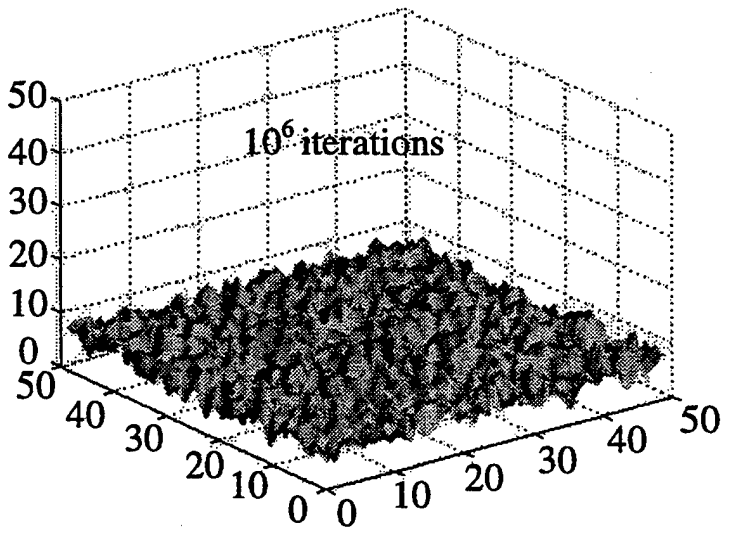

Figure 2a. Evolution of cellular automaton model at 10^6 iterations($\sigma_c = 9$).

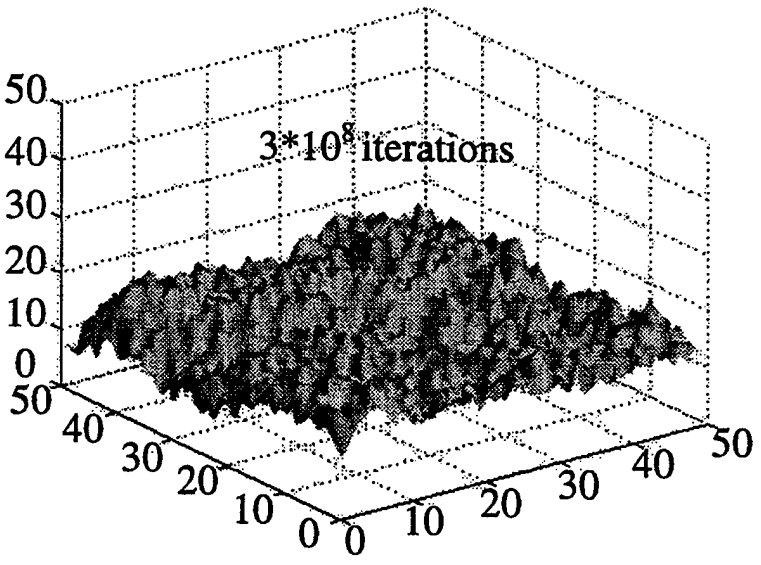

Figure 2b. Evolution of cellular automaton model at $3*10^8$ iterations ($\sigma_c = 9$).

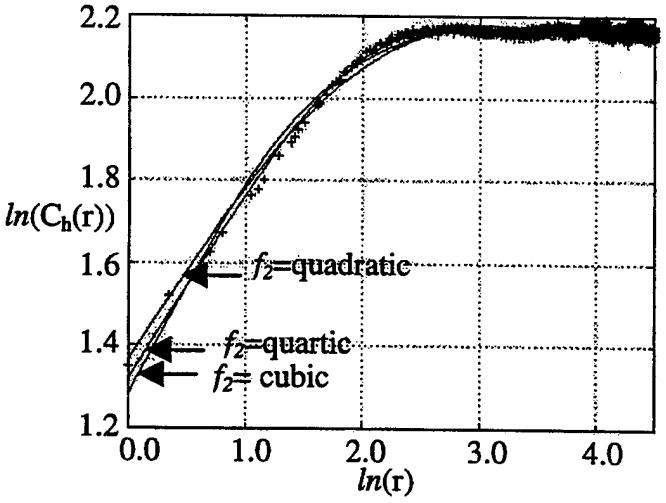

Figure 3. $C_h(r)$ for $\sigma_c = 9$ after 10^7 iterations.

A new systematic procedure has been developed that measures the scaling parameters by fitting linear and polynomial splines to the data and estimating the values of $\xi_{//}$ and H using the data that minimizes the residuals in the fit. The linear range is determined by fitting a straight line, f_1, to the first k points and fitting a polynomial, f_2, to points k through m. k is the index of the data point at which the linear and curved segments meet. It is the variable knot (index) of a linear/curved spline and is a nonlinear parameter determined by exhaustion. m is the index of the data point at which $C_h(r)$ approaches a constant ($\xi_{\perp}$). The value of m is not critical, but should be an estimate of $\xi_{//}$ for computational efficiency. The coefficients of the polynomials are evaluated with continuity enforced at k, and the residuals (ε_i) are computed over the entire range. The value of k for which the residuals are a minimum is selected as the index for the last point of the linear range. k is computed using a quadratic, cubic, and quartic for f_2. C^1 and C^2 continuity are enforced for the quartic fit. C^2 continuity is not enforced for the cubic fit to allow some overshoot in the data. The largest of the three values of k is used to ensure the maximum number of points in the linear region is selected to determine H. If k is less than 3, it is assumed that no linear region exists and that the system does not adhere to fractal theory. $\xi_{//}$ is then determined from the intersection of the linear fit and $\xi_{\perp}$. The points used to compute $\xi_{\perp}$ are at large r where no correlation is observed. The procedure for the quartic fit is outlined below:

$$f_1(x) = a + b(x-k) \tag{7}$$

$$f_2(x) = c + d(x-k) + e(x-k)^2 + f(x-k)^3 + g(x-k)^4 \tag{8}$$

For C^2 continuity at knot k

$$f_1(k) = f_2(k);\ f_1'(k) = f_2'(k);\ f_1''(k) = f_2''(k)$$

and the residuals (ε_i) become

$$\varepsilon_i = a + b\,p_i - y_i \quad for\ i \le i_k$$

$$\varepsilon_i = a + b\,p_i + f\,q_i + g\,r_i - y_i \quad for\ i > i_k$$

where

$$p_i = x_i - k;\ q_i = (x_i - k)^3;\ r_i = (x_i - k)^4 \tag{9}$$

Minimizing the sum of the squares of the residuals S

$$S = \sum_{i=0}^{m} \varepsilon_i^2 = \sum_{LR} \varepsilon_i^2 = \sum_{i=0}^{i_k} \varepsilon_i^2 + \sum_{i=i_{k+1}}^{m} \varepsilon_i^2 = \sum_{L} \varepsilon_i^2 + \sum_{R} \varepsilon_i^2 \tag{10}$$

$$\frac{\partial S}{\partial a} = 0 \Rightarrow a*m + b\sum_{LR} p_i + f\sum_{R} q_i + g\sum_{R} r_i = \sum_{LR} y_i \tag{11}$$

$$\frac{\partial S}{\partial b} = 0 \Rightarrow a\sum_{LR} p_i + b\sum_{LR} p_i^2 + f\sum_{R} p_i q_i + g\sum_{R} p_i r_i = \sum_{LR} p_i y_i \tag{12}$$

$$\frac{\partial S}{\partial g} = 0 \Rightarrow a\sum_{R} r_i + b\sum_{R} p_i r_i + f\sum_{R} q_i r_i + g\sum_{R} r_i^2 = \sum_{R} r_i y_i \tag{13}$$

$$\frac{\partial S}{\partial f} = 0 \Rightarrow a\sum_{R} q_i + b\sum_{R} p_i q_i + f\sum_{R} q_i^2 + g\sum_{R} q_i r_i = \sum_{R} q_i y_i \tag{14}$$

The systems of equations (11) through (14) are solved for coefficients a,b,f, and g for k ranging from 2 to m-1. The data point corresponding to the value of k for which residuals are a minimum is used as the last point in the linear fit. $\xi_{//}$ is then determined from the intersection of the linear fit and $\xi_{\perp}$. In this investigation, k was also computed using a cubic ($g = 0$) and quadratic ($f = g = 0$) for f_2. The largest value of k evaluated using the three different polynomials for f_2 is used in computing H. The following system of equations is solved to determine the coefficients of the cubic and quartic fits for f_2:

Cubic fits:

$$f_2(x) = c + d(x-k) + e(x-k)^2 + f(x-k)^3 \tag{15}$$

$$p_i = x_i - k;\ q_i = (x_i - k)^2;\ r_i = (x_i - k)^3 \tag{16}$$

$$\frac{\partial S}{\partial a} = 0 \Rightarrow a*m + b\sum_{LR} p_i + e\sum_{R} q_i + f\sum_{R} r_i = \sum_{LR} y_i \tag{17}$$

$$\frac{\partial S}{\partial b} = 0 \Rightarrow a\sum_{LR} p_i + b\sum_{LR} p_i^2 + e\sum_{R} p_i q_i + f\sum_{R} p_i r_i = \sum_{LR} p_i y_i \tag{18}$$

$$\frac{\partial S}{\partial e}=0\Rightarrow a\sum_{R}q_i+b\sum_{R}p_iq_i+e\sum_{R}q_i^2+f\sum_{R}q_ir_i=\sum_{R}q_iy_i \tag{19}$$

$$\frac{\partial S}{\partial f}=0\Rightarrow a\sum_{R}r_i+b\sum_{R}p_ir_i+e\sum_{R}q_ir_i+f\sum_{R}r_i^2=\sum_{R}r_iy_i \tag{20}$$

Quadratic fits:

$$f_2(x)=c+d(x-k)+e(x-k)^2 \tag{21}$$

$$p_i=x_i-k;\ q_i=(x_i-k)^2 \tag{22}$$

$$\frac{\partial S}{\partial a}=0\Rightarrow a*m+b\sum_{LR}p_i+e\sum_{R}q_i=\sum_{LR}y_i \tag{23}$$

$$\frac{\partial S}{\partial b}=0\Rightarrow a\sum_{LR}p_i+b\sum_{LR}p_i^2+e\sum_{R}p_iq_i=\sum_{LR}p_iy_i \tag{24}$$

$$\frac{\partial S}{\partial e}=0\Rightarrow a\sum_{R}q_i+b\sum_{R}p_iq_i+e\sum_{R}q_i^2=\sum_{R}q_iy_i \tag{25}$$

Figure 3 shows the intermediate results with 4 points ($k = 4$) in the linear region. The final value of k was 15 using a cubic for f_2 which resulted in the scaling parameters of $H = 0.19$, and $\xi_{//} = 8.08$ for $\xi_{\perp} = 8.76$.

DYNAMIC SCALING HYPOTHESIS

Surface structure in deposition processes is time dependent (ref 7), and a measure of evolving morphology can be obtained by applying a generalization of equation (4) as

$$C_h(\mathbf{r},t)=\left\langle\left[h(\mathbf{r}_0+\mathbf{r},t_0+t)-h(\mathbf{r}_0,t_0)\right]^2\right\rangle_{r_0,t_0} \tag{26}$$

At small t, due to the absence of a characteristic time scale (ref 7), $\xi_{//}$ and $\xi_{\perp}$ are proportional to powers of time t and

$$\xi_{//}(t)\propto t^{1/\zeta}\ for\ t<\tau \tag{27}$$

$$\xi_{\perp}(t)\propto t^{B}\ for\ t<\tau \tag{28}$$

ζ is a conventional exponent for finite size effects, and in general, because of anisotropy in the surface, $1/\zeta \neq B$. τ is the time at which $\xi_{//}$ is equal to the size of the sample. In this investigation, t corresponds to the number of particles added to the system, n.

MPI IMPLEMENTATION

The generalized height correlation function, $C_h(\mathbf{r},t)$, provides useful information about the dynamics of growth processes, but is numerically expensive. Therefore, a suite of homogenous parallel procedures has been developed to map the solution to a multicomputer platform using an implementation of the *Message Passing Interface* (MPI) called LAM (ref 9) for interprocess communication. LAM is a full implementation of the MPI standard, supports heterogeneous computer networks, and provides direct communication between application processes. It is a node-oriented computing environment that uses a unique identifier assigned to each node as the primary synchronization mechanism. The nodes are usually fully connected (maximum 1-hop distance) since the network is generally a shared resource. In our implementation, a master process assigns equal-sized regions of the lattice to slave processing nodes for computation of partial $C_h(\mathbf{r},t)$ data. The processing nodes return the results to the master process where $C_h(\mathbf{r},t)$ is updated and the slave processes assigned new regions to analyze. Although this approach does not exploit the communications advantages of a fully connected network, the load balancing results in a performance improvement directly proportional to the number of workstations. This is likely due to the high computation/communication ratio and the relatively small number of workstations making up the multicomputer.

RESULTS

The dynamics of the evolving surface morphology of the cellular automata models with $\sigma_c = 9$, 10, 11, 13, and 15 on a 256x256 lattice were characterized in terms of the spatial scaling parameters, H, $\xi_{//}$, and $\xi_{\perp}$. The height correlation function was computed at discrete intervals (iterations), and the largest value of k resulting in the minimum residuals using three different polynomials for f_2 was computed. The spatial scaling measures were determined for those surfaces for which fractal theory applied ($k > 2$). These values were used to determine the dynamic scaling exponents $1/\zeta$ and B. Table 1 shows the measured values of H, $\xi_{//}$, and $\xi_{\perp}$ for $\sigma_c = 9$ at each interval and the degree of the polynomial f_2 that resulted in the largest value of k. The table shows that H remains relatively constant as the surface evolves. Results are similar for all other σ_c. In all cases studied, a quartic fit for f_2 resulted in the largest linear region only once.

Table 1. Spatial Scaling Parameters with $\sigma_c = 9$

$N*10^6$	k	f_2	H	$\xi_{//}$	$\xi_{\perp}$
1	3	3	0.16	3.13	5.42
3	7	2	0.17	5.37	6.75
5	12	3	0.17	6.69	7.46
7	13	3	0.18	7.32	8.08
10	15	3	0.19	8.08	8.76
30	19	3	0.21	11.59	10.80
50	33	3	0.22	13.20	12.06
70	26	2	0.22	13.87	12.43
100	37	3	0.22	15.33	12.81
300	35	2	0.23	24.78	16.61

The evolving surface morphologies of the cellular automata models adhere well to the dynamic scaling hypothesis as shown in Figure 4. The figure shows typical *ln-ln* plots of spatial scaling parameters from which the dynamic scaling exponents are derived. The exponents $1/\zeta$ and B are determined from the slope of the straight-line fit using all of the data points. The results for this and the other models are summarized in Table 2. The data show that the value of H increases with increasing σ_c and at any given point in time, the parallel correlation length decreases with increasing σ_c. This result is expected because as σ_c increases, more particles are required for an avalanche to occur. There is no evident correlation between B and σ_c.

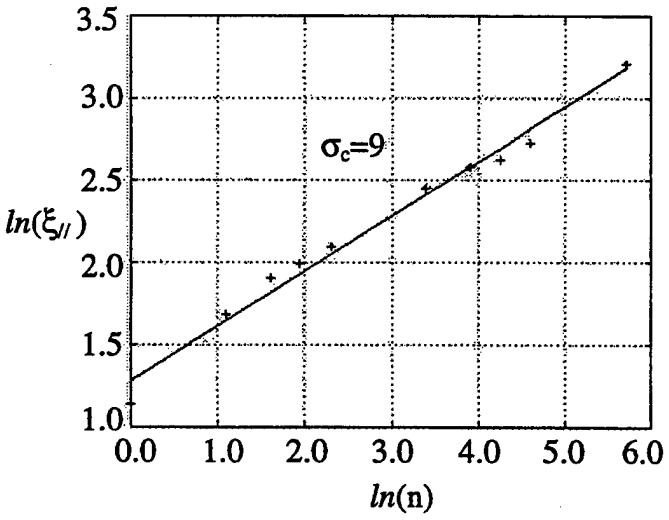

Figure 4. Parallel correlation of length versus time.

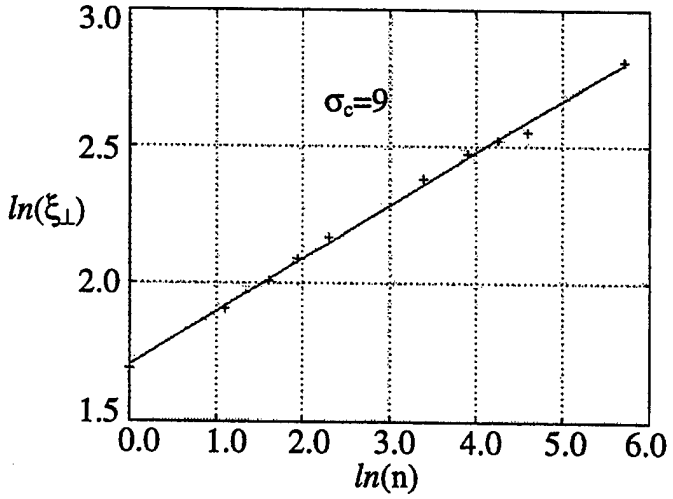

Figure 5. Perpendicular correlation of length versus time.

Table 2. Dynamic Scaling Parameters

σ_c	$\langle H \rangle$	$1/\zeta$	B
9	0.20 ±0.03	0.33	0.19
10	0.25 ±0.04	0.29	0.23
11	0.30 ±0.03	0.27	0.23
13	0.36 ±0.03	0.25	0.24
15	0.41 ±0.01	0.21	0.20

SUMMARY

The deposition of adherent, erosion and corrosion-resistant coatings is critical to the performance of many systems. In order to develop optimal coatings, it is important to understand the effects of changing the parameters controlling the deposition/sputtering processes. Models of the deposition processes and quantitative measures of the condition of the substrate surface and evolving coating are, at present, extremely limited. In this study, cellular automata simulations were used to investigate the nature of the vapor deposition process by exploring the natural evolution of dynamical dissipative systems through self-organized critical system analysis and spatial scaling measures. A new numerical technique was developed to analyze the intrinsic structure of evolving surface morphology in an effort to better understand the dynamics of the growth processes. The algorithm is numerically expensive, therefore the computational problem has been mapped to a multicomputer platform using an implementation of MPI call LAM for interprocess communication. Using this approach, the deposition models were shown to agree well with the dynamic scaling theory. The technique is also being used to validate the integrity of other deposition models through a comparative analysis with experimental data, and to determine if a correlation exists between intrinsic surface structure, evolving surface morphology, and parameters controlling the deposition process.

REFERENCES

1. Bak, P., Tang, C., and Wiesenfeld, K., "Self-Organized Criticality," *Physical Review A*, No. 38, July 1988, pp. 364-374.

2. Kadanoff, L.P., Nagel, S.R., Wu, L., and Zhou, S., "Scaling and Universality in Avalanches," *Physical Review A*, No. 39, June 1989, pp. 6524-6537.

3. Jensen, H.J., Christensen, K.C., and Fogedby, H.C., "1/f Noise, Distribution of Lifetimes, and a Pile of Sand," *Physical Review B*, No. 40, October 1989, pp. 7425-7427.

4. Prado, C.P.C., and Olami Z., "Inertia and Break of Self-Organized Criticality in Sandpile Cellular-Automata Models," *Physical Review A*, No. 45, January 1992, pp. 665-669.

5. Meisel, L.V., and Johnson, M., "Fractal Scaling in Cellular Automata Simulations of Dissipative Dynamical Systems," *Proceedings of 1996 High Performance Computing Symposium*, New Orleans, LA, 8-11 April 1996, SCS, San Diego, CA, pp. 120-124.

6. Pfeifer, P., and Obert, M., *The Fractal Approach to Heterogeneous Chemistry*, (D. Avnir, Ed.) Wiley, NY, 1989, pp. 11-13.

7. Gouyet, J., Rosso, M., and Sapoval, B., *Fractals and Disordered Systems*, (A. Bunde and S. Havlin, Eds.) Springer, Berlin, 1991, pp. 229-234.

8. Mandelbrot B.B., *The Fractal Geometry of Nature*, W.H. Freeman and Company, NY, 1983.

9. Ohio State University, *MPI Primer/Developing with LAM*, Ohio Supercomputer Center, 1224 Kinnear Road, Columbus, OH 43212, 1996.

TECHNICAL REPORT INTERNAL DISTRIBUTION LIST

	NO. OF COPIES
TECHNICAL LIBRARY ATTN: AMSTA-AR-CCB-O	5
TECHNICAL PUBLICATIONS & EDITING SECTION ATTN: AMSTA-AR-CCB-O	3
OPERATIONS DIRECTORATE ATTN: SIOWV-ODP-P	1
DIRECTOR, PROCUREMENT & CONTRACTING DIRECTORATE ATTN: SIOWV-PP	1
DIRECTOR, PRODUCT ASSURANCE & TEST DIRECTORATE ATTN: SIOWV-QA	1

NOTE: PLEASE NOTIFY DIRECTOR, BENÉT LABORATORIES, ATTN: AMSTA-AR-CCB-O OF ADDRESS CHANGES.

TECHNICAL REPORT EXTERNAL DISTRIBUTION LIST

	NO. OF COPIES
DEFENSE TECHNICAL INFO CENTER ATTN: DTIC-OCA (ACQUISITIONS) 8725 JOHN J. KINGMAN ROAD STE 0944 FT. BELVOIR, VA 22060-6218	2
COMMANDER U.S. ARMY ARDEC ATTN: AMSTA-AR-WEE, BLDG. 3022	1
AMSTA-AR-AET-O, BLDG. 183	1
AMSTA-AR-FSA, BLDG. 61	1
AMSTA-AR-FSX	1
AMSTA-AR-FSA-M, BLDG. 61 SO	1
AMSTA-AR-WEL-TL, BLDG. 59 PICATINNY ARSENAL, NJ 07806-5000	2
DIRECTOR U.S. ARMY RESEARCH LABORATORY ATTN: AMSRL-DD-T, BLDG. 305 ABERDEEN PROVING GROUND, MD 21005-5066	1
DIRECTOR U.S. ARMY RESEARCH LABORATORY ATTN: AMSRL-WM-MB (DR. B. BURNS) ABERDEEN PROVING GROUND, MD 21005-5066	1
COMMANDER U.S. ARMY RESEARCH OFFICE ATTN: TECHNICAL LIBRARIAN P.O. BOX 12211 4300 S. MIAMI BOULEVARD RESEARCH TRIANGLE PARK, NC 27709-2211	1
COMMANDER ROCK ISLAND ARSENAL ATTN: SIORI-SEM-L ROCK ISLAND, IL 61299-5001	1
COMMANDER U.S. ARMY TANK-AUTMV R&D COMMAND ATTN: AMSTA-DDL (TECH LIBRARY) WARREN, MI 48397-5000	1
COMMANDER U.S. MILITARY ACADEMY ATTN: DEPT OF CIVIL & MECH ENGR WEST POINT, NY 10966-1792	1
U.S. ARMY AVIATION AND MISSILE COM REDSTONE SCIENTIFIC INFO CENTER ATTN: AMSAM-RD-OB-R (DOCUMENTS) REDSTONE ARSENAL, AL 35898-5000	2
COMMANDER U.S. ARMY FOREIGN SCI & TECH CENTER ATTN: DRXST-SD 220 7TH STREET, N.E. CHARLOTTESVILLE, VA 22901	1

NOTE: PLEASE NOTIFY COMMANDER, ARMAMENT RESEARCH, DEVELOPMENT, AND ENGINEERING CENTER, BENÉT LABORATORIES, CCAC, U.S. ARMY TANK-AUTOMOTIVE AND ARMAMENTS COMMAND, AMSTA-AR-CCB-O, WATERVLIET, NY 12189-4050 OF ADDRESS CHANGES.